J. For. Res. (2020) 31(5):1521–1538
https://doi.org/10.1007/s11676-019-00985-y

ORIGINAL PAPER

Climate and seasonal rainfall anomalies along an elevational gradient in the El Sira Mountains, Peru, and their impacts on tree radial growth

Armin Niessner[1] · Manfred Küppers[1] · James Graham[2] · Luis Valenzuela[3] · Aylin Güney[1] · Sabine Remmele[1] · Reiner Zimmermann[1]

Received: 18 July 2018 / Accepted: 19 September 2018 / Published online: 4 June 2019

Abstract The explicit purpose of this study was to characterize climate and vegetation along the western slope of the El Sira Mountains (Peru) and evaluate radial tree growth in response to seasonal rainfall anomalies. From May 2011 until September 2015, we monitored radial stem growth of 67 trees using point dendrometers and measured climate within five sites along an altitudinal gradient. The transect extends from lowland terra firme forests, over submontane forests, late and mid successional montane cloud forests up to exposed elfin forests. Monthly rainfall estimates by the TRMM PR satellite (product 3B42) were highly correlated with our rain gauge observations but underestimate rainfall at high altitudes. Different intra-annual tree growth patterns could be identified within each elevational forest type, showing species with strictly seasonal growth, continuous growth or alternating growth patterns independent of the seasons. Stem growth at each site was generally larger during rainy seasons, except for the elfin forest. The rainy season from October 2013 to March 2014 was extraordinarily dry, with only 73% of long-term mean precipitation received, which resulted in reduced radial growth, again with the exception of the elfin forest. This indicates that montane tropical rain forests may suffer from prolonged droughts, while exposed ridges with elfin forests still receive plenty of precipitation and benefit from receiving more solar radiation for photosynthesis.

Keywords Cloud forest · Dendrometer · Elfin forest · Seasonality · TRMM PR · Tropical montane forest

Introduction

The Amazon basin is one of the regions of highest rainfall in the world and is a major source for atmospheric water vapor (Figueroa and Nobre 1990). Over the last decades it has experienced a more variable climate, with severe droughts in 2005 and 2010, causing increased tree mortality (Phillips et al. 2009) and reducing carbon uptake (Feldpausch et al. 2016). Some models predict climate-induced Amazon die-back for this century (Salazar et al. 2007; Cox et al. 2008).

Tropical tree growth and, therefore, carbon uptake are linked with atmospheric CO_2 and micro-climate through photosynthesis, while seasonality is mainly determined by the amount of annual rainfall and its seasonal distribution (Borchert 1994). Rising temperatures (Doughty 2011) and reduced dry season rainfall (Clark et al. 2010) reduce photosynthesis through higher leaf-to-air vapor pressure deficits leading to stomatal closure and, thus, limiting carbon uptake, although rising levels of atmospheric CO_2 may compensate for this effect (Lloyd and Farquhar 2008). Studies using remote sensing data, however, analyzed as

---

Project funding: This work was supported by the German Federal Ministry of the Environment, Nature Conservation and Nuclear Safety (BMU), the German Corporation for International Cooperation GmbH (GIZ).

Corresponding editor: Yu Lei.

✉ Armin Niessner
armin.niessner@uni-hohenheim.de

[1] Institute of Botany 210a, University of Hohenheim, Garbenstraße 30, 70599 Stuttgart, Germany

[2] Field Museum, 1400 S. Lake Shore Drive, Chicago, IL 60605, USA

[3] Missouri Botanical Garden, Prolongación Bolognesi Mz. E Lote 6, Oxapampa-Pasco, Peru

MODIS Enhanced Vegetation Index (EVI, an index of canopy photosynthetic capacity) report a 25% increase in photosynthesis between 2000 and 2005 during dry seasons due to more sunlight (Huete et al. 2006). Xiao et al. (2006) suggest that leaf phenology in tropical evergreen forests is not determined by the seasonality of precipitation, but by the availability of solar radiation. A pan-tropical analysis of climate effects on tree growth by Wagner et al. (2014), however, showed that, both, precipitation and solar radiation are the main drivers for seasonal variations in tree growth. Wind disturbance can also be an important ecological force as it may accelerate forest fragmentation (Laurance and Curran 2008). Physiognomy of elfin forests at exposed ridges is an adaptive response to frequently high wind speeds (Lawton 1982).

Neotropical montane rainforests receive some of the highest rainfall, but have received much less scientific attention, associated with difficulties of access due to steep and rugged terrain. Montane rainforests are hot spots of biodiversity and endemism (Gentry 1995) due to altitudinal gradients over more than 2000 m, extraordinary edaphic and micro-climatic heterogeneity, vegetation dynamics due to frequent landslides (Lozano et al. 2007), limitation of nutrients (Homeier et al. 2010) and the landscape history since the Pleistocene (Lauer 1986). Concomitant with increasing altitude on wet tropical mountains, forest structure changes (Von Humboldt 1849) and the altitudinal zonation is even compressed on small outlying mountains (Lomolino 2001). Although the physiognomy of tropical montane forests has been studied for over 100 years (Shreve 1914; Grubb 1977; Martin and Bellingham 2016), it remains poorly understood.

The El Sira Mountains in Peru, an eastern parallel extension of the Andes, reaches into the Amazon basin and forms the first barrier for moist air from the tropical Atlantic and the Amazon basin. It rises up to 2400 m asl, and the windward (eastern) side receives more than 7500 mm rainfall per year (Graham et al. 2016) exceeding annual accumulations for rainfall hotspots over the southern tropical Andes reported by Espinoza et al. (2015). Because of its remote location, rugged terrain and poor accessibility, the El Sira uplands are still covered with true pristine forests and therefore represent an ideal landscape-scale laboratory to investigate the effects of droughts on montane forest ecosystems.

In terms of regional climate patterns, Casimiro et al. (2013) reported that mean annual temperatures increased by 0.09 °C for the Peruvian Amazon-Andes region between 1965 and 2007, but no trend for annual rainfall was presented. Other studies report a decrease in rainfall of 3% per decade for the Mantaro River basin (IGP 2005) and 8.3% per decade for the Peruvian-Ecuadorian Amazon watershed between 1970 and 1997 (Espinoza et al. 2006). Tropical montane regions are generally poorly populated, and networks of rain gauges are sparse or absent, but satellite-based sensors can provide remedy on global scale at remote areas. The "Tropical Rainfall Measuring Mission and Precipitation Radar" (TRMM PR) satellite provides a unique opportunity to examine rainfall characteristics in tropical regions that have low density of observations. It is designed to provide information on the three-dimensional structure of rainfall over the tropics and subtropics (Simpson et al. 1988; Kummerow et al. 2000). Several recent studies have validated satellite rainfall estimates against rain gauge records and strongly supported their applicability (Franchito et al. 2009; Semire et al. 2012; Mantas et al. 2015; Manz et al. 2016).

This study is the first climatological description of an altitudinal gradient on the El Sira uplift and uses TRMM PR rainfall estimates and rain gauge records to identify rainfall anomalies over the last years. In parallel, the effects of seasonal precipitation anomalies on tree radial growth variations are analyzed.

Materials and methods

Study sites

The El Sira Mountains form the backbone of the El Sira Communal Reserve (RC El Sira), located roughly 9°–11° south and 74°–75° west (Fig. 1). It is almost entirely surrounded by lowland Amazonian habitats and isolated from all other Andean elements by large river systems. In the northern and most isolated section of the uplift are found the highest elevations of the entire range, reaching above 2400 m asl.

The study was conducted from May 2011 until September 2015 at an altitudinal gradient along the western slope at the northern part of the mountain range (Fig. 1). Trees selected for observation are located within five permanent 1-ha plots along the gradient established by the RAINFOR project (Malhi et al. 2002; Montegudo et al. 2014; Valenzuela et al. 2015) within the RC El Sira (sites P845-P2230) and the private preserve area "ACP Panguana" (site P251) in the central Amazonia of Peru, region Huanúco (Table 1). Montane rain forest sites within the Communal Reserve are quite remote and only accessible by a 2-day long foot walk, Valenzuela et al. (2015) report at least 729 angiosperm plant species within 120 families and 398 genera for this area. The most abundant families are in this order Orchidaceae, Rubiaceae, Fabaceae, Lauraceae, Melastomataceae and Arecaceae.

Along the transect, different altitudinal forest types can be distinguished (Fig. 2). Tropical lowland rain forests (terra firme) are found between 170 and 650 m asl, tropical

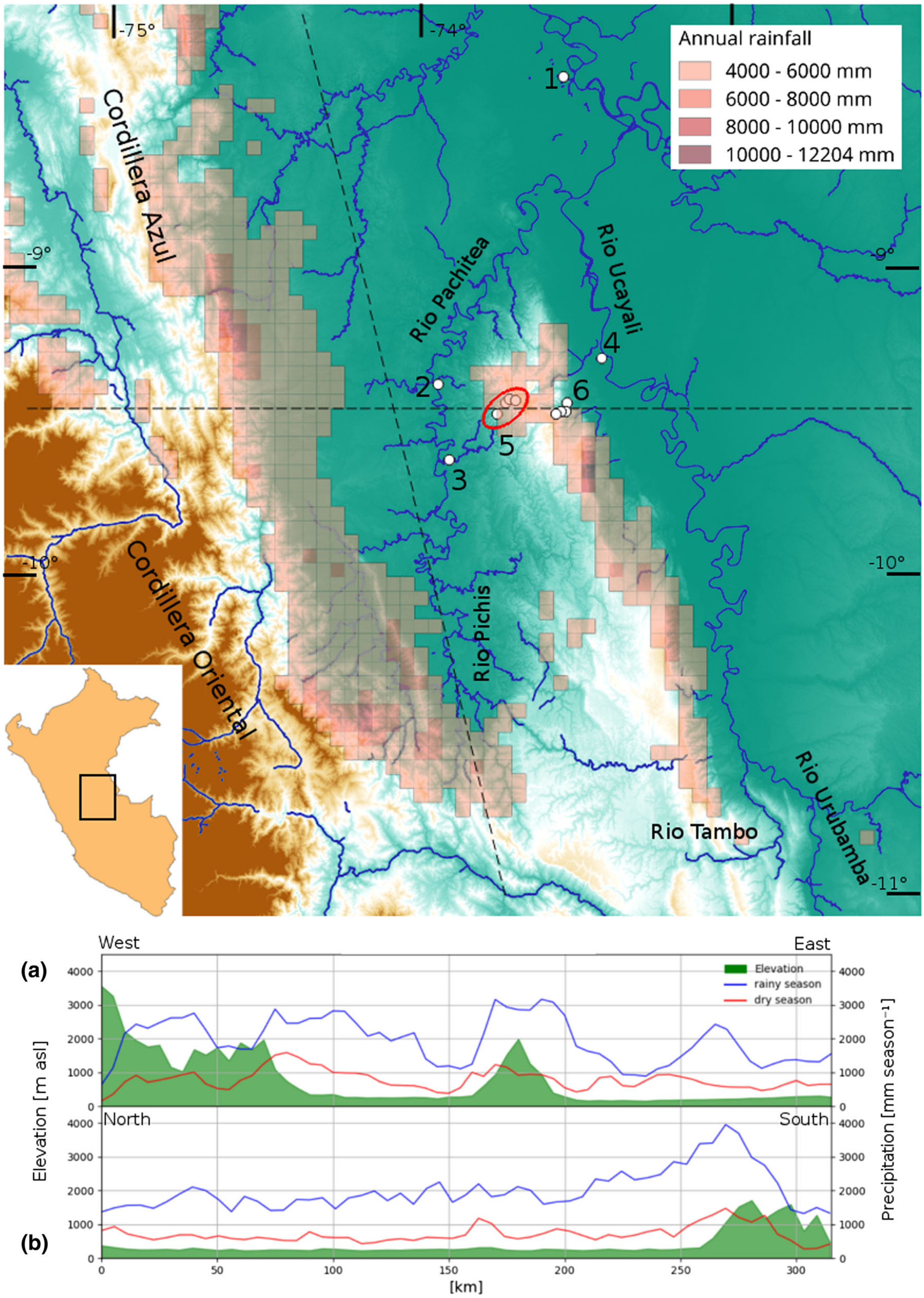

Fig. 1 El Sira cordillera and regional precipitation regimes. The map indicates areas of annual rainfall over 4000 mm (satellite estimates, Manz et al. 2016). 1: Pucallpa, 2: Puerto Inca, 3: Panguana (P251), 4: Iparia, 5 (red oval): Altitudinal transect (P845, P1391, P1568, P2230), 6: Altitudinal transect from Graham et al. 2016. **a**, **b** show topography and seasonal precipitation along horizontal profiles (dashed lines in map) in east–west and north–south direction, respectively

Table 1 Overview of forest sites

Site	Forest type	Location (WGS84)		Altitude (m asl)	Expo-sition	Slope mean incli-nation	Individuals	Families	Genera	Species	Mean DBH (cm)	Max DBH (cm)	Mean height (m)	Max height (m)	Basal area (m^2 ha^{-1})	Bio-mass (t ha^{-1})	Soil
		N	E				(N ha^{-1})	(N ha^{-1})	(N ha^{-1})	(N ha^{-1})							
P251	Lowland	– 9°37′2.208″	– 74°55′46.92″	251	ENE	11	595	44	117	200	19.8 ± 11.3	83.5	13.7 ± 6.2	45	23.23	224.17	Sandy clay, reddish black
P845	Submontane	– 9°28′12.792″	– 74°46′22.44″	845	WNW	14	639	41	86	176	20.3 ± 10.2	69.3	11.9 ± 4.5	27	27.15	264.11	Sandy clay, reddish
P1391	Cloud (ls)	– 9°25′52.572″	– 74°44′41.64″	1391	NW	35	758	39	81	135	18.7 ± 8.7	52.8	11.9 ± 3.7	26	25.53	244.87	70% clay, 30% rocks
P1568	Cloud (ms)	– 9°25′20.136″	– 74°44′4.92″	1568	WSW	22	733	36	60	99	20.9 ± 10.5	116.2	12.6 ± 4.9	25	31.65	233.86	Lime, clay, rocks
P2230	Elfin	– 9°25′28.344″	– 7°42′54.72″	2230	SE	40	483	22	27	46	8.0 ± 2.9	22.7	5.2 ± 1.8	13	2.96	19.37	Humus, mosses, large rocks

Data are taken from Valenzuela et al. (2015) and refer to trees with breast height diameter (DBH) > 10 cm and DBH > 5 cm for the elfin forest. Basal area refers to the sum of cross-sectional areas at breast height and biomass refers to dry matter aboveground. The values after "±" is standard deviation. At Cloud Forests: *ls* late successional, *ms* mid successional

submontane or transitional rain forests between 650 and 1100 m asl, tropical montane cloud forests (TMCF) between 1100 and 1850 m asl and tropical elfin forests (or tropical subalpine forests, Frahm and Gradstein 1991) above 1850 m asl. The occurrence of peat mosses (*Sphagnum* sp.) clearly indicates the perhumid character within elfin forests.

Table 1 shows the location and forest main characteristics of each 1-ha plot. A more comprehensive description of the altitudinal forest types along the transect is given by Valenzuela et al. (2015).

Ground-based climate data

Air temperature (°C), relative air humidity (%), both used to calculate vapor pressure deficit of air (vpd), global solar radiation (W m^{-2}), precipitation (mm), wind direction and speed (m s^{-1}) were recorded every 30 min using Watchdog 2700ET weather stations (Spectrum Technologies, Inc., USA) at 860, 1540 and 2230 m asl, located near to the study sites P845, P1586 and P2230, respectively. The weather station at 860 m ran from August 2011 until August 2015. At 1540 m the station ran only from May 2011 until August 2012 due to an animal attack. The third weather station ran from May 2011 onwards until a lightning stroke in September 2014 destroyed it. Precipitation was measured by tipping buckets but turned out to be inconsistent or even absent for most of the time as a consequence of litter blocking the water discharge of the instrument. Therefore, large cans (volume = 19 L) with funnels collecting rain where additionally installed at the end of March 2015, next to the three weather stations. Total amount of captured rain was measured at the end of August 2015. Long-term rain gauge records of the towns of Pucallpa (154 m asl, about 140 km NE of study area) and Puerto Inca (200 m asl, about 26 km N of study area) were supplied for this study by the National Meteorology and Hydrology Service (SENAMHI, Peru, http://www.senamhi.gob.pe/). The rainy season is defined here as lasting from October until end of March and the dry season from April until end of September.

Remote sensing data

Digital elevation data (SRTM 90 m, from http://srtm.csi.cgiar.org) were used to represent regional topography. In order to illustrate annual precipitation extremes at a 5 × 5 km^2 resolution, we used satellite-borne estimates of precipitation ("TRMM PR product 2A25 version 7", Iguchi et al. 2000, 2009) merged with ground-based rain gauge measurements by a linear model from Manz et al. (2016). For linear regressions of time-series with ground-based rain gauge records we used daily "TRMM PR product 3B42

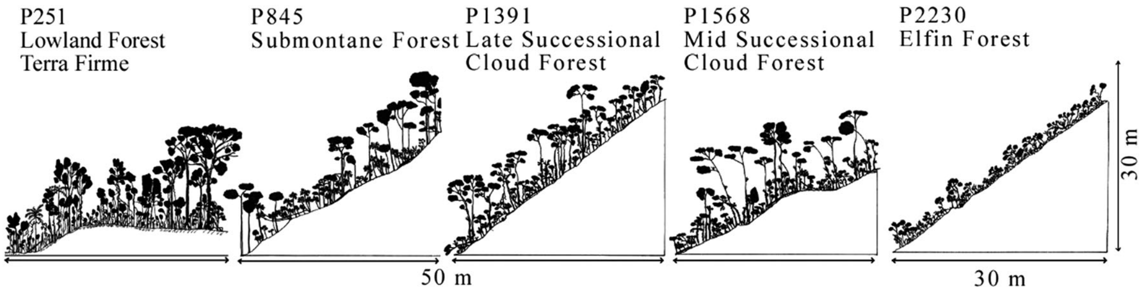

Fig. 2 Vegetational profiles of sites. Depth of projections is about 5 m. For further details see Table 1

version 7" data, which are globally gridded estimates of precipitation compiled from passive-microwave instruments and geosynchronous infrared instruments at a spatial resolution of 0.25° (≈ 28 km for the study area) (Huffman et al. 2007, 2010). GIS data were analyzed and visualized using the open source software "QGIS 2.18.3" and daily rainfall estimates for rain gauge locations were extracted using the "Point Sampling Tool" plugin.

Selection of trees and measurement of radial stem growth

Within each site, 11–15 vital trees of the most frequent species (excluding palms) were selected for observation (Table 2). Identifications and scientific names of species are taken from Montegudo et al. (2014), and complete tree census data are accessible at http://www.forestplots.net/. All selected individuals were equipped with spring-loaded linear displacement potentiometers (MMR 10_11 R5 K, MEGATRON Elektronik AG and Co., Munich, Germany) with a resolution of < 10 µm to detect diurnal and seasonal stem radius changes. Potentiometers were mounted in the center of stainless-steel frames and then fixed to the stem at 1.3 m height with two screws anchored at least 5 cm deep in the xylem, at least 6 cm apart from the measuring point (Güney et al. 2017). They were placed with their tips onto the innermost bark, after partly removing the outer parts without infringing living cortex and cambium, covered and shielded with a reflecting and a plastic foil. Radial changes were recorded every 1-h using a Dl2e datalogger (Delta-T Devices, Cambridge, UK).

Data analysis

Daily stem radius change (src_d) was calculated after Köcher et al. (2012) as the difference between the maximum stem radii in the morning of two subsequent days. Statistical analyses and visualization were carried out in python v.3.5 using the open source packages "pandas", "numpy", "scipy" and "matplotlib". To test for significant differences between src_d during rainy and dry season a Kruskal–Wallis-Test was used. Pearson correlation and linear regression were used to compare daily, monthly and seasonal data of TRMM PR estimates and rain gauge data. Air vapor pressure deficit (vpd) was calculated according to Goff and Gratch (1946). Data gaps are due to sensor or logger failure. Obvious outliers due to malfunctions were deleted.

Results

Regional climate, seasonal patterns and altitudinal gradients

Seasonal precipitation patterns of South America are controlled by the interaction of large-scale atmospheric currents and the complex Andean topography. Along the eastern flanks of the Andes the easterly trade winds and strong topographic gradients generate pronounced orographic effects (Bookhagen and Strecker 2008; Espinoza et al. 2009, 2015) resulting in strong convection (Romatschke and Houze 2010) and thereby spatio-temporally highly intermittent precipitation patterns with precipitation gradients of up to 190 mm km^{-1} (Espinoza et al. 2015). These orographic effects are illustrated in Fig. 1, showing an instant increase in annual rainfall from about 1800 mm at Iparia up to 11,000 mm over the El Sira uplands. Uplands receive up to four times more precipitation during rainy seasons than during dry seasons.

Occasionally cold fronts, advancing from the south along the Andean Mountain Range into the western area of the Amazon basin, let temperatures drop within hours by 10–20 °C (locally called "Friajes"), reaching values of 5–10 °C and generally associated with high wind speeds (Marengo 1983).

The altitudinal gradients in climatic parameters are shown in Fig. 3. From May 2011 until September 2015, temperature (Fig. 3a) ranged from 15.0 °C (July 28, 2013) to 36.1 °C (22 September 2013) in the lowland at Puerto Inca (200 m asl), from 14.6 °C (22 August 2011) to 34.1 °C (22 September 2013) in the submontane forest

Table 2 Overview of monitored trees

Site	RF #	Family	Species	DBH (cm)	Height (m)	src_d ± SD (μm day^{-1})	*N*	src_d ± SD (rainy) (μm day^{-1})	*N*	src_d ± SD (dry) (μm day^{-1})	*N*	src_d ± SD (13/14) (μm day^{-1})	*N*	[1]	[2]	[3]
P251	3496	Malvaceae	*Pachira insignis*	70.8	35	15 ± 56	442	21.1 ± 71	259	6.4 ± 18	179	11.9 ± 76	141	+++	−−−	sr
	3485	Lecythidaceae	*Lecythis pisonis*	83.2	35	14.2 ± 28	366	18.5 ± 24	273	3.2 ± 36	81	18.3 ± 20	94	+++	ns	sr
	3507	Apocynaceae	*Aspidosperma parvifolium*	51.6	34.1	9.4 ± 53	487	7.3 ± 59	298	13.9 ± 39	181	3.8 ± 42	151	ns	−−	c
	3505	Moraceae	*Castilla ulei*	24.9	14.7	8.6 ± 20	439	11.2 ± 15	250	5.1 ± 25	188	8.8 ± 17	133	+++	−−	sr
	3500	Fabaceae	*Ormosia amazonica*	54	25.9	7.7 ± 15	541	10.6 ± 15	340	3.2 ± 13	189	10 ± 16	160	+++	ns	sr
	3369	Chrysobalanaceae	*Hirtella elongata*	34.5	23.4	6.9 ± 9	455	7.9 ± 9	256	6 ± 9	187	9.5 ± 11	77	++	+	cr
	3492	Violaceae	*Leonia glycycarpa*	19.9	14.6	5.6 ± 20	522	5.6 ± 21	324	5.8 ± 18	186	4.1 ± 12	160	ns	ns	−
	3509	Cannabaceae	*Celtis schippii*	27.6	21.3	5.3 ± 53	532	9 ± 35	331	0 ± 75	189	12.4 ± 31	152	+++	+++	sr
	3489	Malvaceae	*Theobroma subincanum*	12.3	10.8	2.2 ± 11	429	2.4 ± 12	278	1.8 ± 10	151	3.4 ± 14	160	ns	ns	−
	3501	Apocynaceae	*Aspidosperma parvifolium*	14.4	15.1	1.3 ± 27	540	1.6 ± 25	339	1.3 ± 29	189	0.4 ± 22	160	ns	ns	−
	3605	Olacaceae	*Aptandra tubicina*	18.5	19	0.8 ± 18	540	1.3 ± 14	339	− 0.2 ± 25	189	0.3 ± 13	160	+	ns	i
	3488	Sapotaceae	*Micropholis egensis*	18.2	11.2	0.3 ± 16	425	0.3 ± 18	251	0.3 ± 13	174	− 0.6 ± 23	134	ns	ns	−
	3495	Malvaceae	*Theobroma cacao*	23	18	0.2 ± 15	478	0.3 ± 15	287	0 ± 17	189	0.3 ± 17	160	ns	ns	−
	3490	Moraceae	*Pseudolmedia laevis*	32	23.4	− 0.2 ± 25	465	1.4 ± 11	277	− 2.6 ± 37	188	1.2 ± 12	160	++	ns	sr
P845	87	Burseraceae	*Dacryodes nitens*	26.8	22.6	12.1 ± 18	883	13.7 ± 21	498	10.1 ± 14	385	8.6 ± 18	155	++	−−−	cr
	365	Sapotaceae	*Chrysophyllum sanguinolentum*	19	21.4	10.4 ± 16	795	14.9 ± 16	367	6.4 ± 15	350	15.9 ± 11	113	+++	ns	sr
	366	Burseraceae	*Dacryodes nitens*	70.3	36.7	7 ± 28	803	9.5 ± 26	357	5 ± 31	363	4.8 ± 22	107	+++	−−	cr
	247	Euphorbiaceae	*Hevea guianensis*	33.6	22.5	6.5 ± 43	573	6.4 ± 21	253	6.6 ± 55	320	0.4 ± 12	172	ns	−−−	sr
	232	Lecythidaceae	*Eschweilera cf. coriacea*	40.6	23	6.1 ± 20	809	6.9 ± 20	424	5.1 ± 19	385	0.8 ± 19	170	ns	−−−	sr
	253	Chrysobalanaceae	*Licania micrantha*	27.5	20.3	6 ± 16	547	7.2 ± 18	256	4.7 ± 15	226	6.7 ± 15	172	ns	ns	c
	219	Malvaceae	*Theobroma subincanum*	17.8	20.8	4.2 ± 17	804	4.8 ± 15	446	1.3 ± 19	275	2.3 ± 15	172	ns	−−	sr
	222	Chrysobalanaceae	*Licania hypoleuca*	20.1	22.5	4 ± 20	913	5.1 ± 21	458	3.5 ± 21	385	2.2 ± 19	172	+	−	i
	227	Lauraceae	*Ocotea ovalifolia*	36.4	28.5	3.8 ± 16	867	7.2 ± 16	401	1.2 ± 14	383	11.5 ± 24	122	+++	++	sr
	363	Malvaceae	*Theobroma subincanum*	14.5	19.1	3.8 ± 23	564	5.3 ± 24	336	1.7 ± 21	228	10.4 ± 26	172	ns	+++	i
	374	Lecythidaceae	*Eschweilera cf. tessmannii*	14.8	19.6	2.9 ± 15	817	4.6 ± 15	440	0.7 ± 13	294	0.2 ± 10	112	+++	−−−	sr
	223	Lecythidaceae	*Eschweilera cf. tessmannii*	30.3	30	2.1 ± 21	937	3.7 ± 20	500	0.1 ± 22	354	− 0.2 ± 25	155	+++	−−−	sr
	403	Lauraceae	*Ocotea* sp.	38.2	22.9	1.7 ± 14	986	1.7 ± 15	518	1.2 ± 14	385	0.8 ± 15	172	ns	ns	i
	376	Burseraceae	*Protium amazonicum*	22.7	20	0.8 ± 31	924	1.7 ± 27	457	0.1 ± 33	385	1.8 ± 27	172	ns	ns	sr
	244	Sapotaceae	*Micropholis guyanensis*	32.9	19.3	0.8 ± 27	931	1.3 ± 30	517	− 0.5 ± 24	331	1 ± 24	172	ns	ns	−

Table 2 continued

Site	RF #	Family	Species	DBH (cm)	Height (m)	src_d ± SD (µm day^{-1})	*N*	src_d ± SD (rainy) (µm day^{-1})	*N*	src_d ± SD (dry) (µm day^{-1})	*N*	src_d ± SD (13/14) (µm day^{-1})	*N*	[1]	[2]	[3]
P1391	1040	Caryocaraceae	*Anthodiscus amazonicus*	54.2	32.5	9.5 ± 19	1454	12.3 ± 24	684	8.7 ± 14	616	8.4 ± 18	141	+++	−	cr
	1390	Moraceae	*Brosimum parinarioides*	34.8	22.3	7.1 ± 11	1481	8.7 ± 13	718	6.9 ± 10	607	3.2 ± 12	174	+++	−−−	sr
	1084	Fabaceae	*Tachigali* sp.	17.4	18.9	6.1 ± 18	975	5 ± 17	361	7 ± 21	460	7.7 ± 20	148	−	+	sd
	1375	Phyllanthaceae	*Hieronyma* sp.	16.4	14.3	4.9 ± 15	1016	4.7 ± 12	536	5.4 ± 13	362	3.1 ± 12	174	ns	−	i
	1250	Cardiopteridaceae	*Dendrobangia boliviana*	25.5	16.3	4.8 ± 12	972	6.6 ± 11	398	4.3 ± 13	430	3.8 ± 7	34	+++	ns	sr
	1382	Chrysobalanaceae	*Licania heteromorpha*	44.4	28.4	3.6 ± 11	1536	4.2 ± 11	718	3.8 ± 12	662	3.3 ± 11	174	++	ns	sr
	1232	Rubiaceae	*Psychotria* sp.	28.3	20.6	3.3 ± 12	807	3.3 ± 12	402	3.4 ± 11	405	4.9 ± 16	152	ns	ns	c
	1036	Lauraceae	*Beilschmiedia* sp.	27.7	18.6	3.1 ± 14	1274	4.3 ± 13	594	1.6 ± 14	626	− 0.5 ± 11	151	+++	−−−	sr
	1041	Cardiopteridaceae	*Dendrobangia boliviana*	52.1	20.8	2.6 ± 8	1259	3.1 ± 8	661	2.5 ± 6	444	1.6 ± 6	159	++	−−−	i
	1192	Moraceae	*Pseudolmedia laevigata*	30.7	20	2.1 ± 11	1265	2.5 ± 11	623	1.8 ± 12	486	2.4 ± 10	174	ns	ns	i
	1355	Sapotaceae	*Pouteria vernicosa*	15.6	15.8	2.1 ± 15	1136	3.6 ± 16	422	1 ± 13	558	2.7 ± 14	113	+++	ns	sr
	1395	Chrysobalanaceae	*Licania heteromorpha*	36.4	34	1.9 ± 14	1251	1.4 ± 13	599	2.6 ± 16	573	− 0.1 ± 10	88	ns	ns	i
	1233	Chrysobalanaceae	*Licania heteromorpha*	21.7	22	1.6 ± 12	1361	1.4 ± 11	699	1.7 ± 12	662	1 ± 12	174	ns	ns	i
	1196	Chrysobalanaceae	*Licania heteromorpha*	27	20	0.5 ± 11	932	0.6 ± 12	471	− 0.3 ± 10	305	0.3 ± 10	109	ns	ns	i
	1005	Cardiopteridaceae	*Dendrobangia boliviana*	45.3	23	0.4 ± 11	1488	0.7 ± 11	708	0 ± 12	624	− 0.1 ± 11	174	ns	ns	i
P1568	1904	Lamiaceae	*Hyptidendron arboreum*	49.3	35.7	17.8 ± 27	1111	21.4 ± 29	430	15.5 ± 25	681	17.9 ± 40	175	+++	−−−	sr
	1905	Melastomataceae	*Meriania hexamera*	24.1	21.3	15.6 ± 15	1132	16.8 ± 13	503	14.6 ± 17	629	23.2 ± 12	150	++	+++	cr
	2013	Lauraceae	*Nectandra* sp.	13.4	13.7	15.2 ± 42	1029	20.5 ± 36	438	11.2 ± 46	591	20.6 ± 29	110	+++	ns	i
	1884	Malvaceae	*Heliocarpus americanus*	41.7	24	10.1 ± 20	1209	11.6 ± 19	528	9 ± 21	681	3.2 ± 15	175	+	−−−	sr
	1879	Fabaceae	*Inga* sp.	13.2	12	9.8 ± 21	1162	15.6 ± 24	484	5.6 ± 16	678	19.3 ± 22	161	+++	+++	sr
	2030	Euphorbiaceae	*Sapium glandulosum*	59.1	32.6	8.8 ± 16	1037	7.6 ± 13	379	9.4 ± 17	658	4.1 ± 11	174	−−	−−−	i
	1713	Lamiaceae	*Hyptidendron arboreum*	37.5	24.3	8.6 ± 22	1186	9.5 ± 23	528	8 ± 20	658	9.7 ± 26	175	ns	ns	i
	2017	Urticaceae	*Cecropia angustifolia*	25.2	17.8	7.7 ± 17	845	6.3 ± 19	309	8.5 ± 16	536	7.3 ± 19	141	ns	ns	i
	1866	Lamiaceae	*Hyptidendron arboreum*	36.5	21	7.5 ± 15	1191	10.6 ± 16	510	5.2 ± 14	681	9.3 ± 17	173	+++	ns	sr
	1854	Phyllanthaceae	*Hieronyma duquei*	12	12.5	2.4 ± 9	1110	4.4 ± 11	476	0.9 ± 6	634	5.3 ± 10	124	+++	ns	sr
	1888	Rubiaceae	*Elaeagia karstenii*	14	9.8	2.2 ± 13	1192	2.5 ± 10	528	2 ± 15	664	2.9 ± 13	175	ns	ns	i
	1893	Urticaceae	*Cecropia angustifolia*	34.8	27.7	1.5 ± 9	1097	1.4 ± 10	420	1.5 ± 8	677	0.1 ± 13	141	ns	ns	i
P2230	2810	Rubiaceae	*Cinchona hirsuta*	13.3	8.1	10 ± 11	662	10.4 ± 11	239	9.9 ± 11	423	12.5 ± 10	180	ns	+++	c
	2808	Araliaceae	*Schefflera patula*	17.3	5.9	5 ± 10	659	4.9 ± 9	246	5 ± 10	413	4.2 ± 8	179	ns	ns	c
	2620	Melastomataceae	*Miconia* sp.	7.6	6.9	3.1 ± 10	378	2.6 ± 10	316	5.8 ± 10	62		176	−	ns	i

Table 2 continued

Site	RF #	Family	Species	DBH (cm)	Height (m)	src_d ± SD (μm day^{-1})	*N*	src_d ± SD (rainy) (μm day^{-1})	*N*	src_d ± SD (dry) (μm day^{-1})	*N*	src_d ± SD (13/14) (μm day^{-1})	*N*	[1]	[2]	[3]
	2827	Rubiaceae	*Cinchona hirsuta*	10	6.8	2.8 ± 13	379	1 ± 9	163	4.1 ± 16	216		0	−−−	ns	sd
	2853	Melastomataceae	*Miconia* sp.	9.8	3.8	2.8 ± 11	270	4.2 ± 17	66	2.4 ± 9	204		0	ns	ns	–
	2809	Araliaceae	*Schefflera patula*	14.3	5.3	2.4 ± 19	742	1.9 ± 18	302	2.7 ± 20	440	2.3 ± 14	180	ns	ns	c
	2819	Araliaceae	*Schefflera patula*	14.3	10.2	1.8 ± 10	783	1.9 ± 10	343	1.6 ± 10	440	2 ± 8	180	ns	ns	c
	2807	Clethraceae	*Clethra castaneifolia*	15.8	8.4	1.5 ± 6	694	1.2 ± 6	260	1.7 ± 7	434	0.7 ± 6	122	ns	ns	i
	2811	Araliaceae	*Schefflera patula*	11.4	7.7	0.9 ± 13	689	0.8 ± 14	343	1 ± 13	346		180	ns	ns	i
	2626	Cunoniaceae	*Weinmannia cochensis*	9.3	5.1	0.4 ± 12	506	0.2 ± 10	285	0.7 ± 15	221		162	ns	ns	i
	2872	Clethraceae	*Clethra castaneifolia*	18.7	7.6	0.3 ± 7	637	0.3 ± 8	301	0.3 ± 7	336	0.1 ± 7	180	ns	ns	i

RF #: given by RAINFOR. Mean daily stem radius changes (src_d) are given for the whole observation period and separately for rainy seasons, for dry seasons and for the rainy season of 2013/14. SD = standard deviation; note: src_d for a given day can also be negative (stem shrinkage) leading to SD being possibly larger than mean src_d, especially during dry periods. *N*: number of days. [1] "+", "++", "+++": src_d for rainy seasons significantly ($p < 0.05$, $p < 0.01$, $p < 0.001$) larger than for dry seasons, and equally "−", "−−", "−−−", if smaller. "ns": not significant. [2] same as [1] but indicating if src_d for the rainy season 2013 was significantly smaller ("−") or larger ("+") than during other rainy seasons. [3] Classification of intra-annual growth pattern, "sr": seasonal growth, predominantly during rainy seasons, "sd": seasonal growth, predominantly during dry seasons, "c": continuous growth, "i": indifferent growth, periods of increment and stagnation regardless of season, "−": identification of growth pattern was not possible due to large data gaps

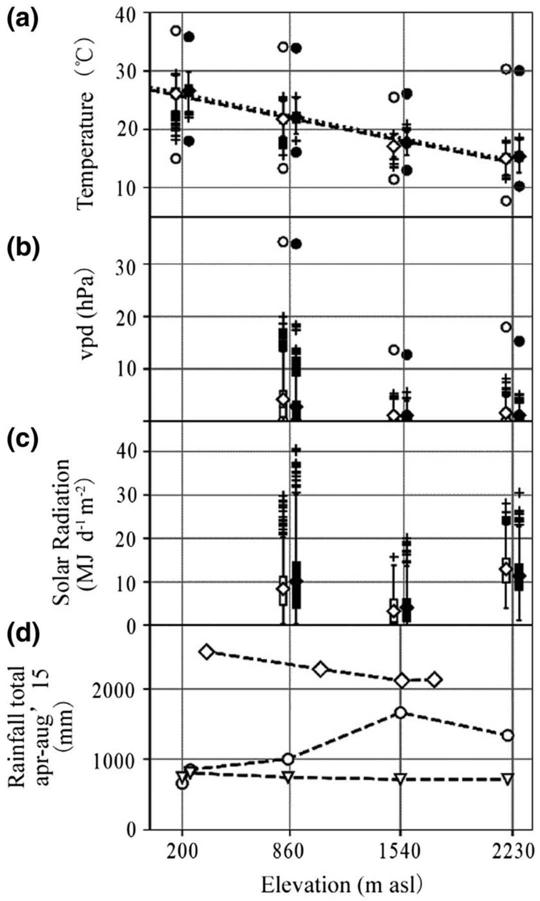

Fig. 3 Altitudinal gradient in climatic parameters. Open boxes and symbols refer to dry seasons (April–September), filled boxes and symbols to rainy seasons (October to March). Boxes indicate the interquartile range (IQR) of daily averages, diamonds represent means, and whiskers extend 1.5 times the IQR from boxes, "+" indicate outliers and circles show absolute extremes. **a** Temperature gradient. Dashed and dotted lines indicate linear regression of average temperature during dry seasons ($y = -0.578/100x + 26.95$, $R^2 = 0.975$, $p = 0.013$) and rainy seasons, respectively ($y = -0.58/100x + 27.43$, $R^2 = 0.978$, $p = 0.011$). Gradients in **b** vapor pressure deficit (vpd) of air, **c** solar radiation, and **d** sum of rainfall between April and August 2015 at the western slope (circles: rain gauges; triangles: TRMM PR estimates) and at the eastern slope (diamonds, Graham et al. 2016)

(860 m asl), and from 7.7 °C (18 July 2012) to 30.3 °C (22 September 2013) in the elfin forest (2230 m asl). Annual mean temperature decreased from 26.5 °C at 200 m asl to 15.1 °C at 2230 m asl (− 0.56 °C per 100 m).

Wind is predominantly blowing from N, NW or E, but during "Friajes" wind is blowing from the S or SE. Mean vpd of air also decreases along the transect (Fig. 3b, diamonds), as a consequence of lower temperatures and cloud formation. The latter leads to a decrease in solar radiation, although exposed upland ridges experience highly variable weather conditions throughout daily courses (Fig. 4) leading to large daily amplitudes in temperature, vpd and solar radiation.

Figure 4 shows three typical days for "sunny", "cloudy/rainy" and "inversion" weather conditions. On the "sunny" day (observed on 1 February 2012), cloud formation was only little, solar radiation exceeded 1000 W m^{-2} at midday, while temperature and vpd exhibited similar daily courses. Dew point temperature (indicating absolute air humidity) varied only little at all sites but decreased with altitude. On the "cloudy/rainy" day (22 February 2012), solar radiation didn't exceed 200 W m^{-2}, air and dew point temperature stayed almost constant throughout the day, vpd was below 4 hPa, with about 122 mm rain measured at P1568 (33 mm at P2230). During the "inversion" day (10 June 2012), the temperature gradient along the transect is inverted (caused by a "Friaje") with cloud formation at lower altitudes. This situation was observed on 42 days (35 of them during dry seasons) and usually lasted for 2–5 days. The temperature drop during these days is predominantly noticeable in lower areas, whereas it is hardly recognizable in the uplands, likely because cold air flows near the ground.

Between April and August 2015, total sum of rainfall increased from 655 mm at Puerto Inca and 849 mm at P251 to 1001 mm at P845 and 1661 mm at P1568 (Fig. 3d, open circles). Towards the peak of the mountain range at P2230, total precipitation appeared to have decreased (1339 mm). The actual amount of rain at the exposed elfin forest site was probably higher but not collected by the rain gauge, as strong winds might have carried rain drops horizontally over the opening of the gauge (Nešpor and Sevruk 1999). In general, precipitation was higher at the eastern slope compared to the western slope (Fig. 3d). Seasonality is particularly noticeable with respect to precipitation, as during rainy seasons total precipitation accounted on average 2.6 times the precipitation of dry seasons (Puerto Inca, 200 m asl, 1993–2009). Mean daily temperatures differed only slightly between seasons, but lowest temperatures were predominantly observed during dry seasons when "Friajes" occurred. During dry seasons, relative air humidity is lower and mean vpd higher. Mean solar radiation at elfin forest ridges is slightly larger during dry seasons likely because there is less water vapor in the air.

Comparison of satellite estimates and ground-based records at the Cordillera El Sira

In contrast to rain gauge observations, satellite based rainfall estimates from TRMM PR exist continuously since 1997 for the research area. Figure 5 shows the monthly precipitation between March 2000 and December 2015 at Puerto Inca. Rain gauge records and TRMM PR satellite estimates are highly correlated (linear regression: $y = 0.83x - 1.43$, $R^2 = 0.72$, $p < 0.001$) and correlation is slightly higher during rainy seasons as compared to dry seasons. TRMM PR estimates mostly overestimate ground-based measurements of Puerto Inca, especially during dry seasons. Maximum seasonal precipitation for both time-series was recorded during the rainy season 2003–2004 (2060 mm gauge and 2084 mm TRMM PR) and minimum was recorded during dry season 2008 (453 mm gauge and 652 mm TRMM PR).

For the altitudinal transect there are only a few months of precipitation records available between 2011 and 2015. Although one grid cell of the TRMM PR data covers about 28 × 28 km^2 and therefore large elevational differences (170–1945 m asl for Puerto Inca and P845, and 170–2443 m asl for P1568 and P2230), monthly precipitations are significantly correlated ($R^2 = 0.74$, $p < 0.01$ at P845 and $R^2 = 0.78$, $p < 0.01$ at P1568), but actual rainfall totals are generally underestimated by TRMM PR estimations (Fig. 6; Fig. 3d, open triangles), as they represent the average rainfall over an area of large elevational differences. Only at 2230 m asl correlation is weak ($R^2 = 0.21$, $p = 0.13$).

A cross-correlation matrix of rain gauge records and TRMM PR estimates for daily, monthly and seasonal data (Table 3) shows that (1) quality of correlations increases from daily over monthly to seasonal records; (2) monthly and daily rain gauge records of Puerto Inca and along the altitudinal gradient are significantly correlated ($p < 0.01$); (3), TRMM PR estimates on seasonal ($p < 0.001$), monthly ($p < 0.01$) and daily ($p < 0.001$) basis are significantly correlated among each other; and (4) rain gauge records and TRMM PR estimates of Pucallpa, which is located about 140 km NE, are significantly correlated with data of our study area. Quantitative info, however, should be taken with caution.

In order to identify rainfall anomalies between 2010 and 2015, deviations from the long-term precipitation pattern between 2000 and 2015 (Fig. 7) are shown in Fig. 8 for Puerto Inca. Deviations calculated on rain gauge and TRMM PR basis are highly significantly correlated ($p < 0.001$) and show excessive rainfall during December 2012 (+ 234 mm for TRMM PR estimates and + 309 mm for rain gauge records). The largest negative deviations were observed during the rainy season from October 2013 to March 2014. Particularly during November 2013 (− 105 mm for TRMM PR and − 70 mm rain gauge), December 2013 (− 176 mm for TRMM PR and − 211 mm rain gauge) and February 2014 (− 214 mm for TRMM PR and − 183 mm rain gauge) it rained unusually little.

The rainy season of 2013/14 was extraordinarily dry, as only 79% according to TRMM PR estimates and only 73% according rain gauge records of long-term mean

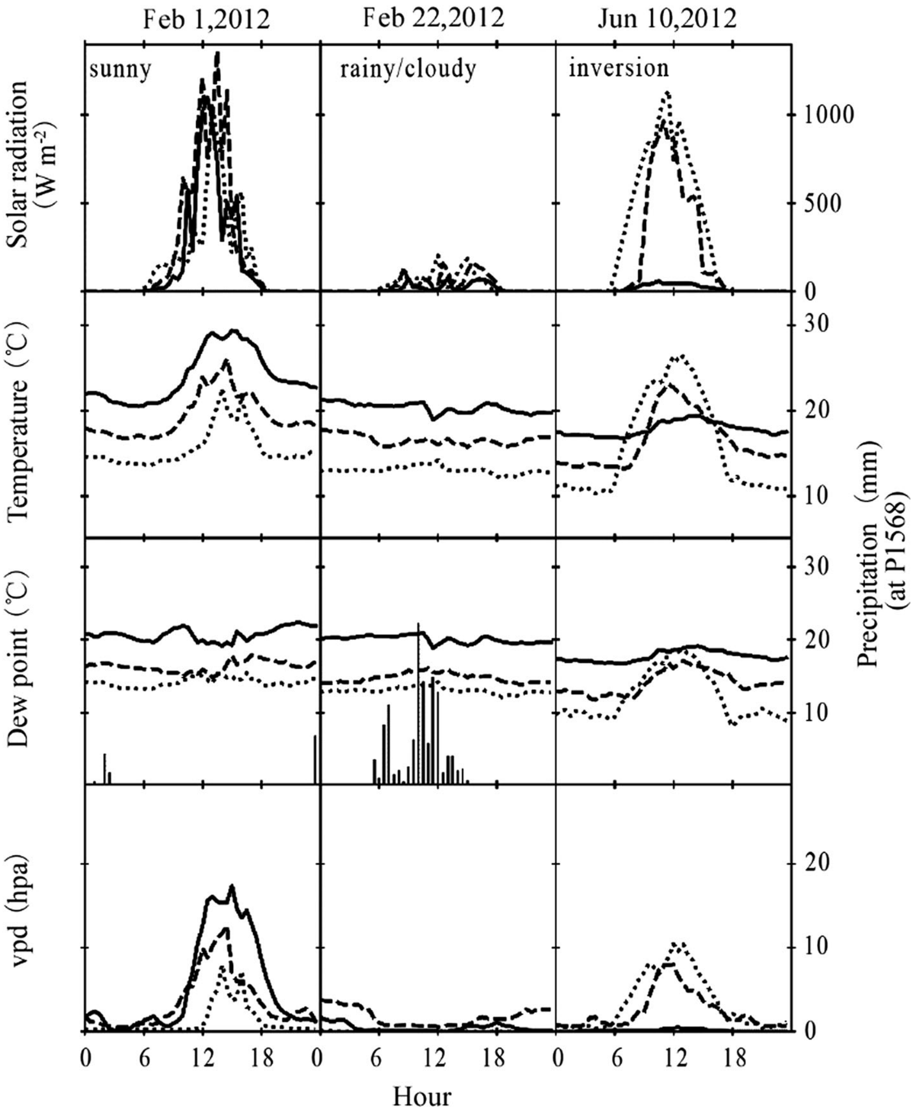

Fig. 4 Daily courses of climate data along the elevational climatic gradient during three selected days ("sunny", "rainy/cloudy", and "inversion"). Altitudes: 860 m (solid lines), 1540 m (dashed lines), and 2230 m (dotted lines). The inversion is predominantly recognizable in air temperature at midday. Daily sums of solar radiation are: 24.1, 19.2 and 13.9 MJ m^{-2} for the "sunny", 2.1, 2.9 and 3.0 MJ m^{-2} for the "cloudy/rainy", and 2.1, 15.7 and 24.4 MJ m^{-2} for the "inversion" day (P845, P1568 and P2230, respectively)

precipitation were received. Obviously, satellite based rainfall estimates can be used to identify precipitation anomalies, but rainfall totals for uplands with large elevational differences should be taken with caution.

Altitudinal gradient of biotic parameters

Altitudinal gradients in climatological parameters lead to floristic, physiognomic, structural and ecological gradients in vegetation (Fig. 9 and Table 1). Tree taxa diversity, diameters at breast height (DBH) and total tree heights

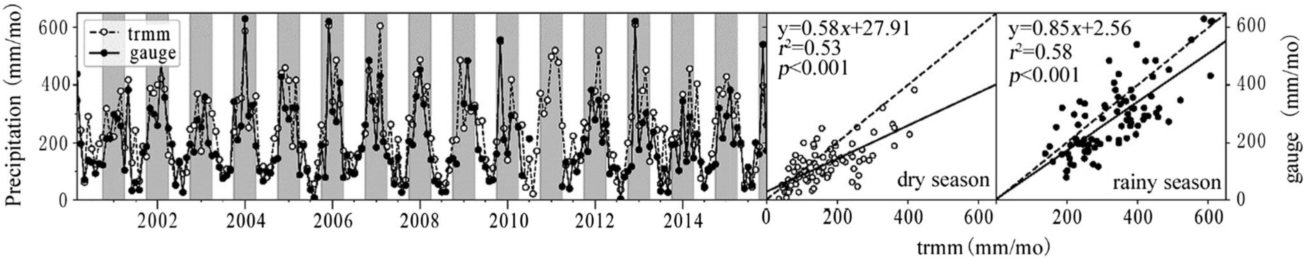

Fig. 5 Comparison of satellite precipitation estimates (TRMM PR 3A42) and ground-based rain gauge measurements for Puerto Inca from March 2000 to December 2015 (left), during dry (middle) and rainy seasons separately (right). Grey shaded areas represent rainy seasons. Dashed lines indicate 1:1 relationships

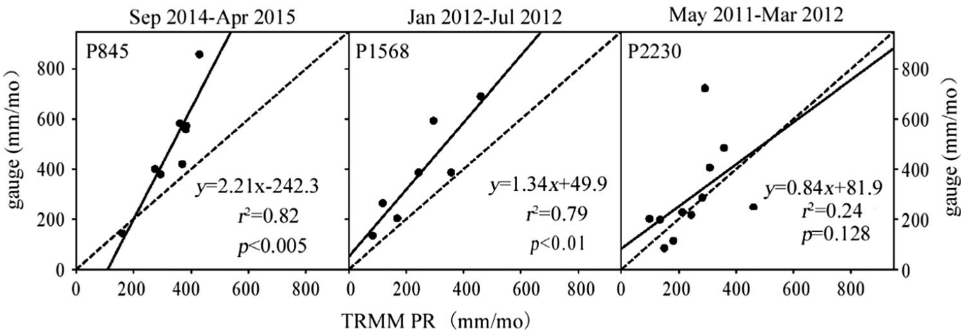

Fig. 6 Comparison of satellite precipitation estimates (TRMM 3A42) and ground-based rain gauge measurements along the elevational gradient. Dashed lines indicate 1:1 relationships

Table 3 Cross-correlation (Pearson) of daily, monthly and seasonal precipitation sums of satellite estimates and rain gauge observations

Parameters			Gauge					TRMM PR	
			Pucallpa	P. Inca	P845	P1568	P2230	Pucallpa	P. Inca, P845
Gauge	P. Inca	Daily	0.30** (1477)						
		Monthly	0.38** (170)						
		Seasonal	0.65** (29)						
	P845	Daily	0.33** (229)	0.62** (229)					
		Monthly	0.20 (8)	0.55 (8)					
		Seasonal	–	–					
	P1568	Daily	0.36** (175)	0.61** (175)	–				
		Monthly	0.43 (6)	0.96* (6)	–				
		Seasonal	–	–	–				
	P2230	Daily	0.23** (337)	0.47** (334)	–	0.71** (63)			
		Monthly	0.65 (11)	0.75* (11)	–	–			
		Seasonal	–	–	–	–			
TRMM PR	Pucallpa	Daily	0.36** (5116)	0.30** (1726)	0.23** (229)	0.33** (175)	0.18** (343)		
		Monthly	0.64** (181)	0.51** (179)	0.09 (8)	0.48 (6)	0.35 (11)		
		Seasonal	0.77** (30)	0.90** (30)	–	–	–		
	P. Inca, P845	Daily	0.16** (5116)	0.60** (1726)	0.49** (229)	0.56** (175)	0.45** (343)	0.43** (5772)	
		Monthly	0.42** (181)	0.85** (179)	0.93** (8)	0.98** (6)	0.51 (11)	0.62** (190)	
		Seasonal	0.69** (30)	0.96** (30)	–	–	–	0.93** (32)	
	P1568, P2230	Daily	0.17** (5116)	0.54** (1726)	0.41** (229)	0.53** (175)	0.42** (343)	0.46** (5772)	0.85** (5772)
		Monthly	0.48** (181)	0.79** (179)	0.86* (8)	0.95* (6)	0.49 (11)	0.66** (190)	0.94** (190)
		Seasonal	0.70** (30)	0.94** (30)	–	–	–	0.96** (32)	0.98** (32)

*$p < 0.01$; **$p < 0.001$; number of observations in parenthesis

decrease with increasing altitude (Fig. 9 a, b, see also Valenzuela et al. 2015). Aboveground dry matter culminates at the pre-montane forest site P845 (Fig. 9c) and total basal area follows the same course, but peaks at the mid-successional cloud forest site P1568. Here the large portion of light wooded pioneer species, predominantly *Heliocarpus americanus* with 14.3%, *Cecropia angustifolia* with 11.3%, *Hyptidendron arboreum* with 4.7% and *Sapium glandulosum* with 1.2% of trees, contributes more to total basal area than to dry matter.

Mean annual radial stem growth decreased with rising elevation from 2.02 mm a^{-1} at the lowland forest site (max = 5.47 mm a^{-1} in *Pachira insignis*, Moraceae), to 1.72 mm·a^{-1} at the submontane forest site (max = 4.43 mm a^{-1} in *Dacryodes nitens*, Burseraceae), 1.44 mm·a^{-1} at the late successional cloud forest site (max = 3.47 mm a^{-1} in *Anthodiscus amazonicus*,

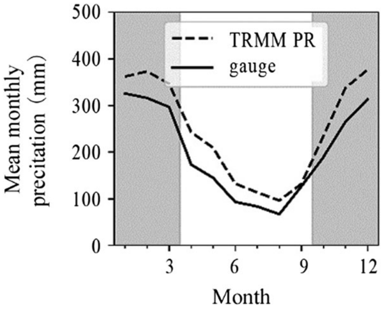

Fig. 7 Mean monthly precipitation at Puerto Inca (2000–2015, 200 m asl), calculated from rain gauge records (solid line) and from TRMM PR rainfall estimates (dashed line). Grey shaded areas represent rainy season

Caryocaraceae) and to 0.97 mm a^{-1} at the elfin forest site (max = 2.97 mm a^{-1} in *Cinchona hirsuta*, Rubiaceae). At the mid successional cloud forest site, however, an exceptionally high mean annual radial growth rate of 3.15 mm a^{-1} (max = 6.5 mm a^{-1} in *Hyptidendron arboreum*, Lamiaceae) was observed due to the high portion of pioneer species.

During dry seasons stems still gain in radius at all sites, but differences between altitudes were not detectable, whereas they were clearly found during rainy seasons as mean radial stem growth decreased by 46 µm per 100 m in altitude (Fig. 9d).

Tree growth patterns in response to season and precipitation anomalies along the altitudinal gradient

Continuous monitoring of radial stem growth permits the identification of different intra-annual growth patterns, shown in Fig. 10 and listed in Table 2. "Seasonal" are trees showing annually repeated periods of radial increment predominantly during rainy seasons ("sr", e.g. *Hieronyma duquei*) or during dry seasons ("sd", e.g. *Tachigali sp.*) followed by a period of stagnation in growth. "Continuous" radial increment ("c") was predominantly, but not exclusively, observed for elfin forest trees, where no stagnation in radial increment was detected (e.g. *Anthodiscus amazonicus*). If radial increment appeared to be continuous but was significantly larger during rainy or dry season the letter "r" or "d" was appended, respectively. "Indifferent", "i", also called "supra-annual" in Newstrom et al. (1994) is defined for trees exhibiting periods of enhanced growth and periods of less or no growth, regardless of seasons (e.g. *Licania heteromorpha*).

The majority of monitored trees could be categorized as "sr" (Tables 2, 4) which were most abundant at the lower sites (P251, P845) and also well represented at the cloud forest (P1391, P1568) but completely absent at the elfin forest (P2230). The second largest group were trees growing "indifferently" ("i") with largest proportions at the cloud and elfin forest sites. "Continuously" ("c" and "cr") growing trees were found at all sites but especially at P2230. Only one tree at each P1391 and P2230 could be categorized as "sd". Trees growing predominantly during rainy seasons ("sr" and "cr") had on average larger stem radial growth rates (src_d) but more than half of them showed significantly ($p < 0.05$) reduced growth rates during the dry rainy season 2013/2014 (column [2] in Table 4). Trees categorized as "i" had on average the smallest src_d and only few were negatively affected (significantly less growth) by the dry rainy season 2013/2014. Most trees (13 out of 19) that were negatively affected by the dry rainy season 2013/2014 were predominantly growing during rainy seasons and present at all sites except for the elfin forest. Here, in contrast to other sites, most individuals (7 out of 11) showed larger radial growth rates during dry seasons, however, but significantly only in trees #2620 (*Miconia sp.*) and #2827 (*Cinchona hirsuta*). Only the latter was categorized as growing seasonally and predominantly during dry seasons ("sd"), all other trees were categorized as "c" or "i".

Considering all trees along the altitudinal transect, respective site means of src_d during rainy seasons was significantly larger than during dry seasons except for the exposed elfin forest (Fig. 11, P2230). The dry rainy season of 2013/2014 significantly decreased src_d as compared to previous and following rainy seasons, although not significantly at P1568. Mean src_d at the elfin forest (P2230) was even larger than during other rainy seasons.

For some species it was possible to monitor more than one individual, as for *Aspidosperma parvifolium* (P251, #3501 and #3507), where only the larger and faster

Fig. 8 Monthly rainfall deviations between 2010 and 2015 from the long-term precipitation regime at Puerto Inca (Fig. 7). Grey shaded areas represent rainy seasons. Correlation of time series: $r^2 = 0.63$, $p < 0.0001$

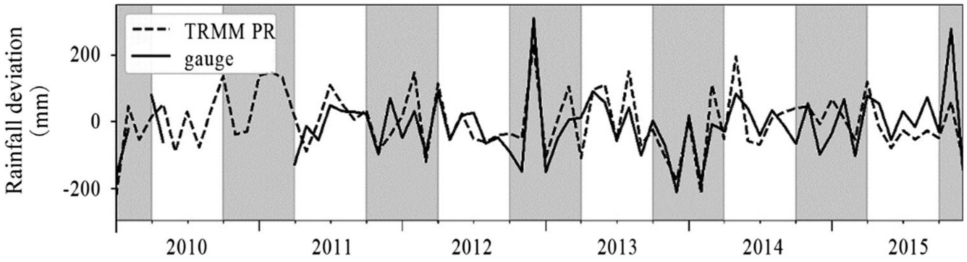

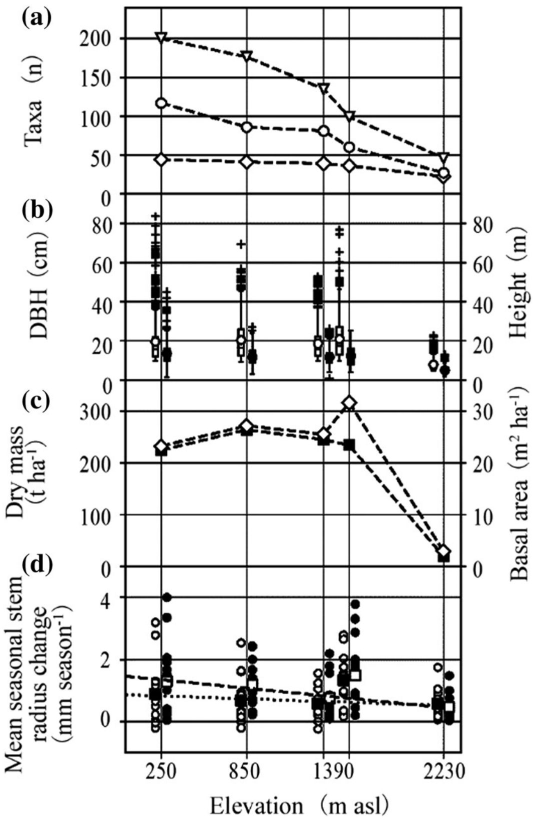

Fig. 9 Altitudinal gradient in vegetation parameters. **a** Number of tree taxa (DBH $\geq$ 10 cm). Triangles: species; circles: genera; and diamonds: families. **b** Boxplots of DBH (open boxes and circles) and tree heights (filled boxes and dots). Boxes indicate the interquartile range (IQR), dots and circles averages, whiskers extend 1.5 times the IQR from boxes, "+" indicate outliers. **c** Above-ground dry biomass (filled squares) and total basal area at breast height (open diamonds). **d** Mean seasonal stem radius change of individual trees during dry seasons (open circles) and rainy seasons (dots). Squares indicate the respective average. Dotted line represents linear regression for dry season ($y = -0.015/100x + 0.866$, $r^2 = 0.77$, $p = 0.12$) and dashed line for rainy season ($y = -0.046/100x + 1.464$, $r^2 = 0.96$, $p = 0.02$). **a**–**c** refer to whole inventory RAINFOR plots of 1 ha

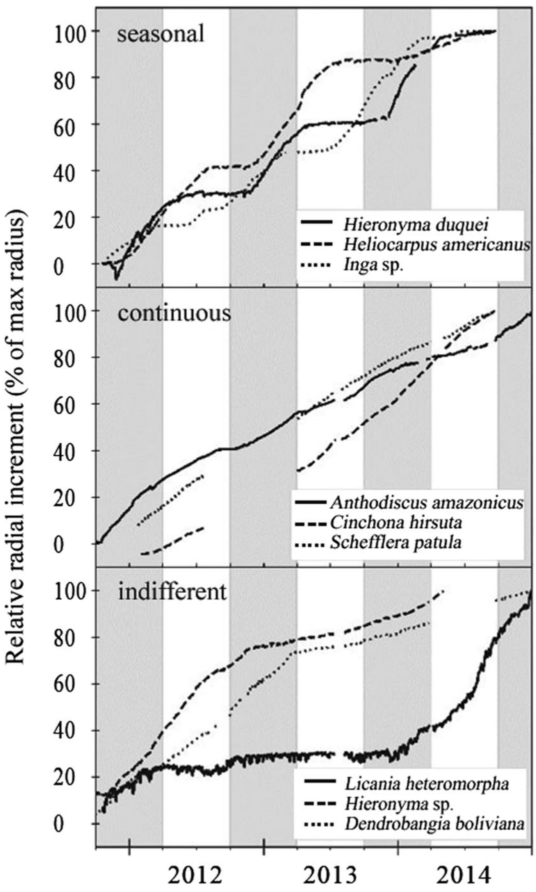

Fig. 10 Examples of intra-annual growth patterns: Strictly "seasonal" growth (predominantly growing during rainy seasons), "continuous" growth throughout seasons without periods of stagnation, and "indifferent" increment, meaning that trees exhibit periods of growth and stagnation, regardless of season. 100% corresponds to the maximum radius measured at the end of observation period. Grey shaded areas represent rainy seasons

growing one (#3507) could be categorized as "c"; its growth was significantly ($p < 0.01$) reduced during rainy season 2013/2014. Individuals of the genus *Eschweilera* (P845, #223, #232 and #374) could all be categorized as "sr" and were significantly ($p < 0.001$) negatively affected by the dry rainy season 2013/2014. Both individuals of *Dacryodes nitens* (P845, #87 and #366) could be identified as "cr" and their growth was significantly ($p < 0.01$) reduced during rainy season 2013/2014. *Licania heteromorpha* (P1391, #1196, #1233, #1382 and #1395) could be categorized as "i", except from the largest and fastest growing individual that had to be identified as "sr". *Dendrobangia boliviana* (P1391, #1005, #1041 and #1250) was also heterogeneous in growth pattern ("i" and "sr") and only growth of the largest individual (#1041) was significantly ($p < 0.001$) reduced during the dry rainy season. Similarly, *Hyptidendron arboreum* (P1568, #1713, #1866 and #1904) could be categorized as "sr" and "i" and, again, only the largest and fastest growing individual showed a significant ($p < 0.001$) growth reduction during rainy season 2013/2014.

Discussion

Applicability of satellite rainfall estimates for the El Sira uplands

Central Amazonian montane forests are poorly populated and accessibility is limited or in the case of El Sira extremely difficult. Therefore, networks of meteorological stations are sparse or absent, but space-borne precipitation measurements could overcome this lack of information.

Bookhagen and Strecker (2008) used the TRMM PR 2B31 product with higher spatial (5 × 5 km^2) but lower

Table 4 Overview of seasonal growth patterns and distribution along the transect

Group	n	src_d ± SD (µm day^{-1})	[1]	[2]	P251	P845	P1391	P1568	P2230
sr	24	6.5 ± 4.6	20	11	6	8	5	5	0
cr	5	11.1 ± 3.7	5	4	0	2	1	1	0
c	7	5.6 ± 3.1	0	0	1	1	1	0	4
i	21	3.4 ± 3.8	4	4	1	2	7	6	5
sd	2	4.4 ± 2.4	0	0	0	0	1	0	1
sum	59	–	29	19	8	13	15	12	10
[1]	29	7.3 ± 5.0	–	13	8	7	7	7	0
[2]	19	7.5 ± 4.3	13	–	3	8	5	3	0

[1] Number of individuals growing significantly ($p < 0.05$) more during rainy seasons, and [2] growing significantly ($p < 0.05$) less during the rainy season 2013/2014 as compared to "normal" rainy seasons. P251 to P2230 indicate number of individuals found per site. This table summarizes Table 2

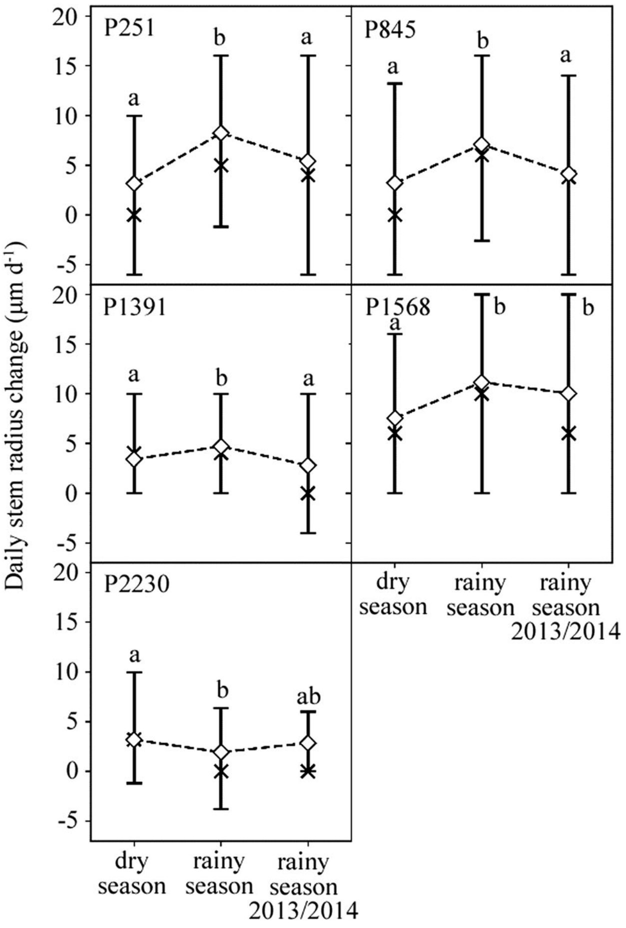

Fig. 11 Stem radial change in µm day^{-1} (src_d) of all trees at the respective site during dry seasons, rainy seasons and the rainy season of 2013/2014 (October to March). Vertical bars: interquartile range of src_d; Cross: median; Diamond: mean. Different letters indicate significant differences at $p < 0.01$

temporal resolution in order to analyze rainfall gradients along the eastern flank of the Andes, although Espinoza et al. (2015) report that TRMM PR (2B25) underestimates rainfall by 35 percent in rainfall hotspot regions. Manz et al. (2016) reported low performance and high uncertainty for areas with low and intermittent precipitation regimes (e.g. the Peruvian Pacific coast).

On the other hand, rain gauge measurements represent only point source estimates of actual rainfall, as observations on small scales can differ largely within a landscape especially at low rainfall intensities (Habib et al. 2001; Ciach 2003). At exposed sites of high wind speeds, rain drops may be carried horizontally over the openings of rain gauges and may not be recorded (Nešpor and Sevruk 1999) thus actual rainfall is underestimated.

Our study shows that the TRMM PR 3B42 product generally overestimated total rainfall at Puerto Inca (200 m asl) east of the Cordillera El Sira but underestimated rainfall along the altitudinal gradient, likely as a consequence of its low spatial resolution. One grid cell covers an area of about 28 × 28 km^2 and includes areas between 170 and 2443 m asl, therefore it represents the average over a large elevational gradient. However, temporal variations in rainfall on daily and monthly basis were well correlated along the transect and between rain gauge observations and satellite estimates (Table 4). It could be shown that the TRMM PR 3B42 product can be used to identify monthly and seasonal rainfall anomalies for the study area as was done for the unusually dry rainy season from October 2013 to March 2014.

Radial tree growth along tropical elevational gradients

Plant species diversity (Gentry 1988; Lieberman et al. 1996; Aiba and Kitayama 1999; Kessler 2002), tree stature (Grubb 1977; Cavelier 1996; Lieberman et al. 1996; Aiba and Kitayama 1999) and radial tree growth (Bräuning et al. 2008) generally decrease concomitant with higher elevation above sea level. Reduced tree growth can be partly explained by changes in species composition, since most fast growing pioneer species occur at lower altitudes

(Homeier 2004), but it can also be a consequence of limited nutrient supply (Soethe et al. 2008), since lower temperatures, reduced transpiration (Küppers et al. 2008) and water-saturated soils inhibit mineralization. Furthermore, it is reported that leaf area index decreases with altitude (Moser et al. 2007; Unger et al. 2013), associated with lower canopy carbon gains and an increase in root to shoot ratio (Leuschner et al. 2007). The consequence is that less assimilated carbon is invested in aboveground biomass, leading to reduced stem growth. Additionally, Graham et al. (2003) reported that frequent cloud cover limits growth of rainforest trees, reducing radiation for photosynthesis. Motzer et al. (2005) and Küppers et al. (2008) demonstrated for montane tropical trees that stomatal conductance and transpiration are reduced which in turn lead to reduced sap flow.

The radial growth rates reported here are generally comparable with data reported for other tropical lowland and montane forests. For moist lowland forests in Panama, Lang and Knight (1983) reported annual diameter growth rates of 0–11.5 mm, Clark et al. (2003) noted 0.9–14.1 mm a^{-1} for Costa Rica and Laurance et al. (2004) measured between 0.25–7.01 mm a^{-1} in Brazil. Within the lowland forest site P251, we report a mean annual diameter growth between 4.04 and 10.94 mm.

Growth rates in tropical montane cloud forests are generally lower, e.g., Herwitz and Young (1994) reported diameter growth rates of 2.7 mm a^{-1} at montane rain forests in Australia, Bellingham and Tanner (2000), however, only measured rates between 0.4–0.9 mm a^{-1} in Jamaica. We observed means of 3.44 mm (submontane forest, P845) and 2.88 mm (montane cloud forest, P1391), although at the pioneer dominated cloud forest site (P1568) an exceptionally high average of 6.3 mm a^{-1} was measured.

Growth rates in tropical elfin forests are rather small, with rates of only 0.3 mm a^{-1} (Weaver et al. 1986) and 0.25 mm a^{-1} (Walker et al. 1996) both reported for elfin forests in Puerto Rico. The elfin forest site sampled here (P2230) showed growth rates of 1.84 mm a^{-1}, which is comparable to those reported by Holder (2008) with 2.0 mm a^{-1} in Guatemala.

Seasonal growth and drought sensitivity of radial increment along the altitudinal gradient

Over the last decades the Amazon basin has experienced several prolonged droughts (particularly in 2005 and 2010) which resulted in increased tree mortality (Phillips et al. 2009) and reduced carbon uptake (Feldpausch et al. 2016). Tropical montane rainforests, however, generally receive vast amounts of rainfall throughout the year and rarely experience severe soil water deficits (Lyford 1969; Herrmann 1971; Kapos and Tanner 1985; Bruijnzeel et al. 1993).

Our study indicates that both, trees of lowland and montane cloud forests predominantly grow during rainy seasons, and that the exceptionally dry rainy season from October 2013 to March 2014 reduced tree growth even in montane cloud forests. Seasonally growing trees tend to be more sensitive to droughts during rainy seasons and were more abundant at lower sites but completely absent from the elfin forest. These trees are presumably adapted to high rainfall amounts during rainy seasons and seasonal variability in growth is dependent on seasonal allocation of carbohydrates. We assume that most seasonal growing trees are mainly flowering and fruiting during dry seasons, being partly defoliated (reliably observed for *Ocotea ovalifolia* P845, #227*)*. They concentrate their vegetative growth on rainy seasons when rainfalls are abundant and usually reliably frequent. The onset of growth may be synchronized with first heavy rainfalls and replenished soil water content; when, however, rainfalls stay absent radial growth will be delayed and prolonged dry periods lead to stem shrinkage and restrict stem growth.

At the elfin forest, in contrast, radial stem growth was comparatively larger during dry seasons and was particularly enhanced during the dry rainy season of 2013/2014. This is likely a consequence of reduced cloud immersion and, therefore, increased solar radiation available for photosynthesis (Graham et al. 2003). Soils of elfin forest formations in the uplands of the El Sira Communal Reserve are generally water-saturated, due to high annual rainfalls, and trees rarely experience severe droughts limiting radial increments.

Within lower altitudes and up to cloud forest formations at about 1500 m asl along the western slope of the northern El Sira uplift, however, prolonged droughts limit stem radial increments. Therefore, future shifts in species composition along the El Sira uplift may be a consequence of more frequent and/or intense droughts over the century, since many neotropical taxa are restricted to wet areas (Esquivel-Muelbert et al. 2016).

Within single taxa, detected growth pattern was not necessarily homogenous, but larger individuals tend to have larger growth rates and growth was more reduced during the dry rainy season 2013/2014. Additional information on wood anatomy could complement studies on drought sensitivity of trees as vessel diameter and frequency drives vulnerability to stem hydraulic dysfunction through embolized vessels (Tyree et al. 1994). Large vessels permit a high stem water flow and high canopy transpiration rates, allowing on the one hand high rates of carbon assimilation if sufficient soil water is available. On the other hand, the hydraulic system is more vulnerable to failure through water stress-induced embolism, leading to stem shrinkage and restricting stem radial growth. Small vessels can limit water supply to leaves during phases of high solar radiation and a high vpd, forcing stomata to reduce conductance, by this limiting carbon assimilation, however, vessels are less susceptible to water stress-induced embolism. Therefore, data on anatomy has been collected and will be presented in a future study.

Conclusion

Satellite estimates of precipitation with high temporal and low spatial resolution, like the TRMM PR 3B42 product, can be applied to identify monthly and seasonal rainfall anomalies. Quantitative estimates should be taken with caution at areas of large elevational differences within small distances, as for the Cordillera El Sira.

The rainy season from October 2013 to March 2014 at Puerto Inca was exceptionally dry with only 73% (79% for TRMM) of the mean seasonal precipitation.

Cold fronts from the south advancing into the western areas of the Amazon basin (locally called "Friajes") do not affect uplands above 1500 m asl at the Cordillera El Sira.

Various radial tree growth patterns along the altitudinal gradient were identified (seasonal, continuous and indifferent growth). Stem growth during rainy seasons was generally larger than during dry season at all sites except from the elfin forest site. Trees within the elfin forest at about 2230 m asl predominantly exhibited a continuous increment throughout seasons.

The exceptionally dry rainy season of 2013/2014 resulted in reduced radial growth of trees at all, but the elfin forest site. Here, trees appear to profit of fewer cloud immersion and thus radial increment was enhanced and similar to growth rates during dry seasons. Seasonal growing trees tend to be more sensitive to droughts during rainy seasons.

Acknowledgements The authors would like to thank the German Federal Ministry of the Environment, Nature Conservation and Nuclear Safety (BMU), the German Corporation for International Cooperation GmbH (GIZ) and the former head of the project Alois Kohler for the logistical and financial support which allowed us to conduct regular expeditions to the El Sira. We thank Juliane Diller, head of the ACP Panguana, Carlos Vásquez and family at Panguana station, for their hospitality and support. We also thank SERNANP el Sira and staff for cooperation and help along the altitudinal transect and the Peruvian Ministry of Environment (MINAM).

References

Aiba S, Kitayama K (1999) Structure, composition and species diversity in an altitude-substrate matrix of rain forest tree communities on Mount Kinabalu, Borneo. Plant Ecol 140:139–157

Bellingham PJ, Tanner EVJ (2000) The influence of topography on tree growth, mortality, and recruitment in a tropical montane forest. Biotropica 32:378–384

Bookhagen B, Strecker MR (2008) Orographic barriers, high-resolution TRMM rainfall, and relief variations along the eastern Andes. Geophys Res Lett 35:L06403

Borchert R (1994) Water status and development of tropical trees during seasonal drought. Trees 8:115–124

Bräuning A, Homeier J, Cueva E et al (2008) Growth dynamics of trees in tropical mountain ecosystems. In: Beck E, Bendix J, Kottke I et al (eds) Gradients in a tropical mountain ecosystem of Ecuador. Springer, Berlin, pp 291–302

Bruijnzeel LA, Waterloo MJ, Proctor J et al (1993) Hydrological observations in montane rain forests on Gunung Silam, Sabah, Malaysia, with special reference to the 'Massenerhebung' effect. J Ecol 81:145–167

Casimiro WS, Labat D, Ronchail J et al (2013) Trends in rainfall and temperature in the Peruvian Amazon-Andes basin over the last 40 years (1965–2007). Hydrol Process 27:2944–2957

Cavelier J (1996) Environmental factors and ecophysiological processes along altitudinal gradients in wet tropical mountains. In: Mulkey SS, Chazdon RL, Smith AP (eds) Tropical forest plant ecophysiology. Springer US, Boston, pp 399–439

Ciach GJ (2003) Local random errors in tipping-bucket rain gauge measurements. J Atmos Ocean Technol 20:752–759

Clark DA, Piper SC, Keeling CD, Clark DB (2003) Tropical rain forest tree growth and atmospheric carbon dynamics linked to interannual temperature variation during 1984–2000. Proc Natl Acad Sci 100:5852–5857

Clark DB, Clark DA, Oberbauer SF (2010) Annual wood production in a tropical rain forest in NE Costa Rica linked to climatic variation but not to increasing CO_2. Glob Chang Biol 16:747–759

Cox PM, Harris PP, Huntingford C et al (2008) Increasing risk of Amazonian drought due to decreasing aerosol pollution. Nature 453:212–215

Doughty CE (2011) An in situ leaf and branch warming experiment in the Amazon. Biotropica 43:658–665

Espinoza JC, Fraizy P, Guyot JL et al (2006) La variabilité des débits du Rio Amazonas au Pérou. Climate variability and change-hydrological impacts, 424–429. IAHS Publ 308:424–429

Espinoza JC, Ronchail J, Guyot JL et al (2009) Spatio-temporal rainfall variability in the Amazon basin countries (Brazil, Peru, Bolivia, Colombia, and Ecuador). Int J Climatol 29:1574–1594

Espinoza JC, Chavez S, Ronchail J et al (2015) Rainfall hotspots over the southern tropical Andes: spatial distribution, rainfall intensity, and relations with large-scale atmospheric circulation. Water Resour Res 51:3459–3475

Esquivel-Muelbert A, Baker TR, Dexter KG et al (2016) Seasonal drought limits tree species across the Neotropics. Ecography (Cop) 39:1–12

Feldpausch TR, Phillips OL, Brienen RJW et al (2016) Amazon forest response to repeated droughts. Global Biogeochem Cycles 30:964–982

Figueroa SN, Nobre CA (1990) Precipitation distribution over central and western tropical South America. Climanalise 5:36–45

Frahm J-P, Gradstein SR (1991) An altitudinal zonation of tropical rain forests using byrophytes. J Biogeogr 18:669–678

Franchito SH, Rao VB, Vasques AC et al (2009) Validation of TRMM precipitation radar monthly rainfall estimates over Brazil. J Geophys Res 114:D02105

Gentry AH (1988) Changes in plant community diversity and floristic composition on environmental and geographical gradients. Ann Mo Bot Gard 75:1–34

Gentry AH (1995) Patterns of diversity and floristic composition in neotropical montane forests. In: Churchill SP, Baslev H, Forero

E, Luteyn JL (eds) Biodiversity and conservation of neotropical montane forests: proceedings. New York Botanical Garden, Bronx, pp 103–126

Goff JA, Gratch S (1946) Low-pressure properties of water from −160 to 212°F. In: 52nd annual meeting of the American Society of Heating and Ventilating Engineers. New York, pp 95–122

Graham EA, Mulkey SS, Kitajima K et al (2003) Cloud cover limits net CO2 uptake and growth of a rainforest tree during tropical rainy seasons. Proc Natl Acad Sci 100:572–576

Graham JG, Fischer M, Pócs T (2016) Bryoflora and landscapes of the eastern Andes of central Peru : I. Liverworts of the El Sira Communal Reserve. Acta Biol Planatarum Agriensis 4:3–60

Grubb PJ (1977) Control of forest growth and distribution on wet tropical mountains: with special reference to mineral nutrition. Annu Rev Ecol Syst 8:83–107

Güney A, Küppers M, Rathgeber C et al (2017) Intra-annual stem growth dynamics of Lebanon Cedar along climatic gradients. Trees 31:1375

Habib E, Krajewski WF, Kruger A (2001) Sampling errors of tipping-bucket rain gauge measurements. J Hydrol Eng 6:159–166

Herrmann R (1971) Die zeitliche Änderung der Wasserbindung im Boden unter verschiedenen Vegetationsformationen der Höhenstufen eines tropischen Hochgebirges (Sierra Nevada de Sta Marta/Kolumbien) (Temporal Change in Soil Moisture Potential under Different Vegetation Format). Erdkunde 25:90–102

Herwitz SR, Young SS (1994) Mortality, recruitment, and growth rates of montane tropical rain forest canopy trees on Mount Bellenden-Ker, Northeast Queensland, Australia. Biotropica 26:350–361

Holder CD (2008) Diameter growth and decline in a tropical montane cloud forest of the Sierra de Las Minas, Guatemala. J Trop For Sci 20:292–299

Homeier J (2004) Baumdiversität, Waldstruktur und Wachstumsdynamik zweier tropischer Bergregenwälder in Ecuador und Costa Rica. Schweizerbart Science Publishers, Stuttgart

Homeier J, Breckle S-W, Günter S et al (2010) Tree diversity, forest structure and productivity along altitudinal and topographical gradients in a species-rich Ecuadorian montane rain forest. Biotropica 42:140–148

Huete AR, Didan K, Shimabukuro YE et al (2006) Amazon rainforests green-up with sunlight in dry season. Geophys Res Lett 33:2–5

Huffman GJ, Bolvin DT, Nelkin EJ et al (2007) The TRMM multisatellite precipitation analysis (TMPA): quasi-global, multiyear, combined-sensor precipitation estimates at fine scales. J Hydrometeorol 8:38–55

Huffman GJ, Adler RF, Bolvin DT, Nelkin EJ (2010) The TRMM multi-satellite precipitation analysis (TMPA). In: Gebremichael M, Hossain F (eds) Satellite rainfall applications for surface hydrology. Springer, Dordrecht, pp 3–22

IGP (2005) Vulnerabilidad Actual y Futura ante el Cambio Climático y Medidas de Adaptación en la Cuenca del Río Mantaro

Iguchi T, Kozu T, Meneghini R et al (2000) Rain-profiling algorithm for the TRMM precipitation radar. J Appl Meteorol 39:2038–2052

Iguchi T, Kozu T, Kwiatkowski J et al (2009) Uncertainties in the rain profiling algorithm for the TRMM precipitation radar. J Meteorol Soc Jpn Ser II 87A:1–30

Kapos V, Tanner EVJ (1985) Water relations of jamaican upper montane rain forest trees. Ecology 66:241–250

Kessler M (2002) The elevational gradient of Andean plant endemism: varying influences of taxon-specific traits and topography at different taxonomic levels. J Biogeogr 29:1159–1165

Köcher P, Horna V, Leuschner C (2012) Environmental control of daily stem growth patterns in five temperate broad-leaved tree species. Tree Physiol 32:1021–1032

Kummerow C, Simpson J, Thiele O et al (2000) The status of the tropical rainfall measuring mission (TRMM) after two years in orbit. J Appl Meteorol 39:1965–1982

Küppers M, Motzer T, Schmitt D et al (2008) Stand structure, transpiration responses in trees and vines and stand transpiration of different forest types within the mountain rainforest. In: Beck E, Bendix J, Kottke I et al (eds) Gradients in a tropical mountain ecosystem of Ecuador. Springer, Berlin, pp 243–258

Lang GE, Knight DH (1983) Tree growth, mortality, recruitment, and canopy gap formation during a 10-year period in a tropical moist forest. Ecology 64:1075–1080

Lauer W (1986) Die Vegetationszonierung der Neotropis und ihr Wandel seit der Eiszeit. Plant Biol 99:211–235

Laurance WF, Curran TJ (2008) Impacts of wind disturbance on fragmented tropical forests: a review and synthesis. Austral Ecol 33:399–408

Laurance WF, Nascimento HEM, Laurance SG et al (2004) Inferred longevity of Amazonian rainforest trees based on a long-term demographic study. For Ecol Manag 190:131–143

Lawton RO (1982) Wind stress and elfin stature in a montane rain forest tree: an adaptive explanation. Am J Bot 69:1224–1230

Leuschner C, Moser G, Bertsch C et al (2007) Large altitudinal increase in tree root/shoot ratio in tropical mountain forests of Ecuador. Basic Appl Ecol 8:219–230

Lieberman D, Lieberman M, Peralta R, Hartshorn GS (1996) Tropical forest structure and composition on a large-scale altitudinal gradient in Costa Rica. J Ecol 84:137–152

Lloyd J, Farquhar GD (2008) Effects of rising temperatures and [CO_2] on the physiology of tropical forest trees. Philos Trans R Soc B Biol Sci 363:1811–1817

Lomolino M (2001) Elevation gradients of species-density: historical and prospective views. Glob Ecol Biogeogr 10:3–13

Lozano PC, Bussmann RW, Küppers M (2007) Montane forest diversity influencing pioneer flora on natural landslides at the Western side of Podocarpus National Park, South Ecuador. Rev UDO Agrícola 7:142–159

Lyford WH (1969) ecology of an elfin forest in Puerto Rico. 7. Soil, root, and earthworm relationships. J Arnold Arbor 50:210–224

Malhi Y, Phillips OLL, Lloyd J et al (2002) An international network to monitor the structure, composition and dynamics of Amazonian forests (RAINFOR). J Veg Sci 13:439–450

Mantas VM, Liu Z, Caro C, Pereira AJSCJSC (2015) Validation of TRMM multi-satellite precipitation analysis (TMPA) products in the Peruvian Andes. Atmos Res 163:132–145

Manz B, Buytaert W, Zulkafli Z et al (2016) High-resolution satellite-gauge merged precipitation climatologies of the tropical Andes. J Geophys Res Atmos 121:1190–1207

Marengo J (1983) Estudio sinoptico-climatico de los Friajes (Friagems) en la Amazonia Peruana. Rev For del Perú 12:1–26

Martin PH, Bellingham PJ (2016) Towards integrated ecological research in tropical montane cloud forests. J Trop Ecol 32:345–354

Montegudo AL, Valenzuela Gamarra L, Vásquez Martínez R et al (2014) Primer catálogo de los árboles y afines de la Reserva Comunal El Sira, Perú. Arnaldo 21:127–164

Moser G, Hertel D, Leuschner C (2007) Altitudinal change in LAI and Stand leaf biomass in tropical montane forests: a transect study in Ecuador and a pan-tropical meta-analysis. Ecosystems 10:924–935

Motzer T, Munz N, Küppers M, Schmitt D, Anhuf D (2005) Stomatal conductance, transpiration and sap flow of tropical montane rain forest treesin the southern Ecuadorian Andes. Tree Physiol 25:1283–1293

Nešpor V, Sevruk B (1999) Estimation of wind-induced error of rainfall gauge measurements using a numerical simulation. J Atmos Ocean Technol 16:450–464

Newstrom LE, Frankie GW, Baker HG (1994) A new classification for plant phenology based on flowering patterns in lowland tropical rain forest trees at La Selva, Costa Rica. Biotropica 26:141–159

Phillips OL, Aragao LEOC, Lewis SL et al (2009) Drought sensitivity of the Amazon rainforest. Science (80-) 323:1344–1347

Romatschke U, Houze RA (2010) Extreme summer convection in South America. J Clim 23:3761–3791

Salazar LF, Nobre CA, Oyama MD (2007) Climate change consequences on the biome distribution in tropical South America. Geophys Res Lett 34:2–7

Semire FA, Mohd-Mokhtar R, Ismail W et al (2012) Ground validation of space-borne satellite rainfall products in Malaysia. Adv Space Res 50:1241–1249

Shreve F (1914) A montane rain-forest: a contribution to the physiological plant geography of Jamaica. Carnegie Institution of Washington, Washington

Simpson J, Adler RF, North GR (1988) A proposed tropical rainfall measuring mission (TRMM) satellite. Bull Am Meteorol Soc 69:278–295

Soethe N, Wilcke W, Homeier J et al (2008) Plant growth along the altitudinal gradient—role of plant nutritional status, fine root activity, and soil properties. In: Beck E, Bendix J, Kottke I et al (eds) Gradients in a tropical mountain ecosystem of Ecuador. Springer, Berlin, pp 259–266

Tyree MT, Cochard H, Davis SD (1994) Biophysical perspectives of xylem evolution: is there a tradeoff of hydraulic efficiency for vulnerability to dysfunction? IAWA J 15:335–360

Unger M, Homeier J, Leuschner C (2013) Relationships among leaf area index, below-canopy light availability and tree diversity along a transect from tropical lowland to montane forests in NE Ecuador. Trop Ecol 54:33–45

Valenzuela L, Vásquez Martínez R, Rojas Gonzáles R del P et al (2015) Línea base para el monitoreo de la vegetación en la Reserva Comunal El Sira (RCS) Baseline for screening the vegetation of El Sira Comunal Reserve. Arnaldo 22:243–268

Von Humboldt A (1849) Aspects of nature, in different lands and different climates; with scientific elucidations. Translated by M. Sabine. Longman, Brown, Green and Longman, London

Wagner F, Rossi V, Aubry-Kientz M et al (2014) Pan-tropical analysis of climate effects on seasonal tree growth. PLoS ONE 9:20–22

Walker LR, Zimmerman JK, Lodge DJ, Guzman-Grajales S (1996) An altitudinal comparison of growth and species composition in hurricane-damaged forests in Puerto Rico. J Ecol 84:877–889

Weaver PL, Medina E, Pool D et al (1986) Ecological observations in the dwarf cloud forest of the Luquillo Mountains in Puerto Rico. Biotropica 18:79–85

Xiao X, Hagen S, Zhang Q et al (2006) Detecting leaf phenology of seasonally moist tropical forests in South America with multi-temporal MODIS images. Remote Sens Environ 103:465–473